

Entanglement generated by dissipation

Hanna Krauter^{1*}, Christine A. Muschik^{2*}, Kasper Jensen¹, Wojciech Wasilewski¹, Jonas M. Petersen¹, J. Ignacio Cirac², and Eugene S. Polzik¹.

¹*Niels Bohr Institute, Danish Quantum Optics Center QUANTOP, Copenhagen University, Blegdamsvej 17, 2100 Copenhagen Denmark.*

²*Max-Planck-Institut für Quantenoptik, Hans-Kopfermann-Strasse, D-85748 Garching, Germany*

**These authors contributed equally to this work.*

Entanglement is not only one of the most striking features of Quantum Mechanics but also an essential ingredient in most applications in the field of Quantum Information. Unfortunately, this property is very fragile. In experiments conducted so far, coupling of the system to a quantum mechanical environment, commonly referred to as dissipation, either inhibits entanglement or prevents its generation. In this Letter, we report on an experiment in which dissipation induces entanglement between two atomic objects rather than impairing it. This counter-intuitive effect is achieved by engineering the dissipation by means of laser- and magnetic fields, and leads to entanglement which is very robust and therefore long-lived. Our system consists of two distant macroscopic ensembles containing about 10^{12} atoms coupled to the environment composed of the vacuum modes of the electromagnetic field. The two atomic objects are kept entangled by dissipation at room temperature for about 0.015s. The prospects of using this method to obtain extremely long-lived entanglement in a steady state are discussed.

Up to date, all experiments investigating quantum superpositions and entanglement are hampered by decoherence. Its effects have been studied in several systems [1–6]. However, it was recognized [7] that if the interaction with a reservoir can be engineered, the system will be driven into a desired steady state. Furthermore, if two or more systems interact with the same environment, this common dissipation can drive them into an entangled state [8–11]. For sufficiently strong interaction, the generated entanglement is robust against other sources of noise and can live, in principle, for an arbitrarily long time. Hence, the production of entanglement by dissipation is not only an intriguing phenomenon, but it also paves the way towards the realization of long-lived entanglement which, in turn, is expected to play a crucial role in quantum information protocols [12–16].

In atomic ensembles, entanglement has been generated either by measurements [17–22] or by atomic interactions [23, 24] and has been inhibited by dissipation, often dominated by the coupling of the atoms to the vacuum modes of the electromagnetic field. However, if two ensembles share certain spontaneous emission modes of the e.-m. field, and the coupling is engineered, dissipation can lead to an entangled state. This is the central idea implemented in this Letter. In contrast to previous experiments [15–20] where the dissipation-limited entanglement life time did not exceed 1ms [16], our scheme does not require detection of light. The dissipative interaction can be understood in terms of a continuous measurement by the environment which produces the desired quantum state independently of the possible measurement outcomes.

Fig. 1 presents two atomic samples with $N \gg 1$ atoms, which interact with a laser field and the vacuum modes of the electromagnetic field. The basic entangling mechanism can be understood by considering the vacuum modes in the direc-

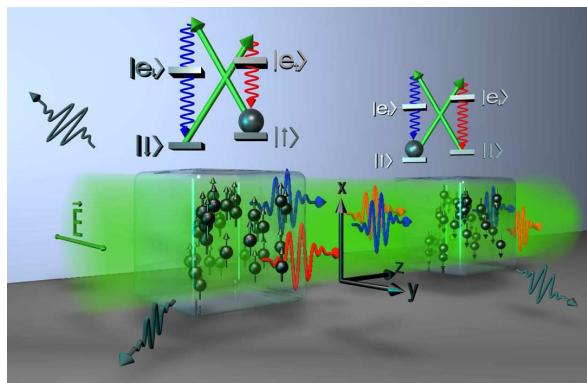


Figure 1: Setup: two spatially separated atomic ensembles interact with the environment composed of the vacuum modes of the electromagnetic field. The coupling is driven by the \hat{y} -polarized laser beam (green shade) propagating in the \hat{z} direction. The engineered collective dissipation is due to photons scattered in the forward direction. Internal level scheme of the atoms in the ensemble: Electronic ground-state levels $|\uparrow\rangle$ and $|\downarrow\rangle$ are Zeeman-shifted by a magnetic field applied in the \hat{x} direction, which defines the quantization axis. Atoms in the two ensembles are initialized in the opposite spin states. The laser beam off-resonantly couples these levels to the excited states, $|e_{\uparrow}\rangle$ and $|e_{\downarrow}\rangle$ and to the electromagnetic vacuum modes. Due to the Zeeman shift of the ground state levels, photons are emitted into the upper and lower sideband (shown in blue and red color) centered around $\omega_L + \Omega$ and $\omega_L - \Omega$, where Ω is the Zeeman splitting and ω_L is the frequency of the applied laser field.

tion of the laser field with wave-vector \mathbf{k}_L and the rest of the modes separately. The latter give rise to the standard spontaneous emission. The former are shared by both ensembles and provide therefore the desired common environment. As emission into the forward direction is collectively enhanced for a large optical depth d [16], these modes can successfully compete with all the others.

Fig. 1 also shows the internal-level structure of atoms with two ground states $|\uparrow\rangle$ and $|\downarrow\rangle$ and illustrates the interaction of the forward-scattered modes with the two ensembles described by a Hamiltonian of the type $H \propto \int_{\Delta\omega_{ls}} d\mathbf{k} (Aa_{\mathbf{k}}^\dagger + A^\dagger a_{\mathbf{k}}) + \int_{\Delta\omega_{us}} d\mathbf{k} (Ba_{\mathbf{k}}^\dagger + B^\dagger a_{\mathbf{k}})$. Here, $a_{\mathbf{k}}^\dagger$ is the creation operator for a photon with wave vector \mathbf{k} ; the first and second integral cover narrow bandwidths $\Delta\omega_{ls}$ and $\Delta\omega_{us}$ centered around the lower (red) and upper (blue) sideband respectively; $A = \mu J_I^- + \nu J_{II}^+$, $B = \mu J_{II}^- + \nu J_I^+$, where J_{iII}^\pm denote collective spin operators, and $J^- = \frac{1}{\sqrt{N}} \sum_{i=1}^N |\uparrow\rangle_i \langle\downarrow|$, $J^+ = \frac{1}{\sqrt{N}} \sum_{i=1}^N |\downarrow\rangle_i \langle\uparrow|$. μ and ν are proportional to the transition amplitudes associated with the emission of photons into the red and blue sideband in the first ensemble (and vice versa in the second one) and are determined by the corresponding Clebsch-Gordan coefficients. As usual, $J_y = \frac{1}{2}(J^+ + J^-)$ and $J_z = \frac{i}{2}(J^+ - J^-)$. The modes give rise to dissipative dynamics governed by the following master equation (see Supplementary Information):

$$\frac{d}{dt}\rho = d \frac{\Gamma}{2} (A\rho A^\dagger - A^\dagger \rho A + B\rho B^\dagger - B^\dagger \rho B + H.C.) + \mathcal{L}_{\text{noise}}\rho,$$

where ρ is the density operator of the ensembles, and Γ is the single atom radiative decay. The terms in parentheses drive the system into a state with $\xi < 1$ [25], which certifies the creation of an inseparable state [17, 26]. Here, $\xi = \Sigma_J / (2\langle J_x \rangle) = (\mu - \nu)^2$, and $\Sigma_J = \text{var}(J_{y,I} + J_{y,II}) + \text{var}(J_{z,I} - J_{z,II})$. $\mathcal{L}_{\text{noise}}$ describes undesired processes such as standard spontaneous emission, collisions with the walls, etc. Remarkably, for sufficiently optically thick samples, the creation of entanglement in a steady state is possible even in the presence of these noise processes (see Eq. (4) of the Methods).

The experiment is performed using ^{133}Cs vapor in two glass cells in a special spin preserving setup [27]. The two-level system $|\uparrow\rangle_{I/II}$ and $|\downarrow\rangle_{I/II}$ is encoded in the $6S_{1/2}$ ground state sublevels $|F = 4, m_F = \pm 4\rangle$ and $|F = 4, m_F = \pm 3\rangle$ in the first and second ensemble respectively. A bias magnetic field of 0.9G leads to a Zeeman splitting of $\Omega = 322\text{kHz}$, corresponding to the frequency shift of the red and blue sidebands from the carrier frequency ω_L . The two ensembles are initialized in the states $|4, \pm 4\rangle$ with orientation $P > 0.995$ by applying a pump laser polarizing the $F = 4$ manifold and a laser repumping atoms from $F = 3$ to $F = 4$ for 15ms. (see Supplementary Information for characterization of this process). At time $t = 0$ the pump- and repump fields are turned off. The paraffin-based coating of the cells and careful magnetic shielding lead to the non-radiative decoherence time for populations and coherences of $T_1 = 0.13\text{s}$ and $T_2 = 0.04\text{s}$, respectively. The dissipation mechanism is engaged by applying a \hat{y} -polarized $5 \div 15\text{mW}$ driving laser blue detuned by 850MHz from the $F = 4 \leftrightarrow F = 5$ component of the D_2 line corresponding to $(\mu - \nu)^2 = 0.16$ for the geometry shown in Fig. 1. The single atom spontaneous emission reduces T_2 to 6ms and T_1 to 34ms. This decoherence has been considered the fundamental limitation for the entanglement generated by

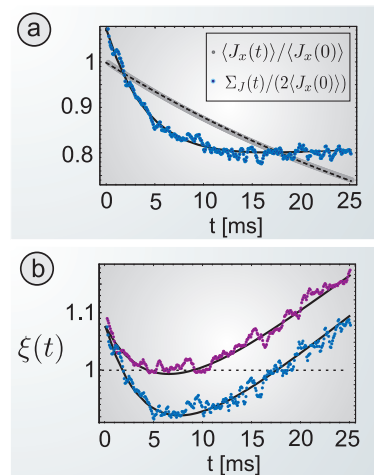


Figure 2: Entanglement generated by dissipation. a) Time evolution of $\Sigma_J(t) / (2\langle J_x(0) \rangle)$ (shown in blue) and $\langle J_x(t) \rangle / \langle J_x(0) \rangle$ (depicted in grey). The fits (full and dashed black line) are based on the parameters $d = 50$ (optical density), $\Gamma_{\text{col}} = 0.004$ (collisional rate) and $\bar{\Gamma} = 0.127$ (dephasing rate), as detailed in the Supplementary Information. The rates for driving field induced transitions $|\downarrow\rangle \rightarrow |\uparrow\rangle$ and $|\uparrow\rangle \rightarrow |\downarrow\rangle$ are given by $\mu^2\Gamma_L$ and $\nu^2\Gamma_L$ respectively, where $\Gamma_L = 0.001$. b) Entanglement $\xi(t)$ versus time in ms. Blue data points correspond to the results shown in a). Violet points show results obtained for a lower atomic density and therefore lower optical depth ($d = 30$). The other parameters used in the fits take the same values as in a). $\xi(t) < 1$ certifies the creation of an inseparable state.

measurements [16]. In the present experiment, the collective entangling dissipation due to forward scattering (see Fig. 1) dominates over the single atom decoherence and leads to a rapid reduction of $\Sigma_J(t)$. Fig. 2a shows the time evolution of $\Sigma_J(t)$ normalized to $2\langle J_x(0) \rangle$. For a coherent spin state $\xi = 1$, and $\Sigma_{\text{CSS}} = 2\langle J_x \rangle$ defines the projection noise (PN) level, below which lies the noise level of entangled states. The dynamics of $2\langle J_x(t) \rangle$ due to single atom spontaneous emission and collisions on the slow time scale of T_1 is also shown in Fig. 2a. Fig. 2b presents the amount of produced entanglement $\xi = \Sigma_J(t) / (2\langle J_x(t) \rangle) < 1$ for two values of the optical depth $d = 30$ and $d = 50$. For $d = 50$, the entanglement generated by dissipation can be created and maintained even though the initial atomic noise $\Sigma_J(0)$ is significantly above the PN level. This property is a special feature of the dissipative evolution, which drives the system into an entangled state independent on the initial state. The maximum entanglement $\xi = 0.92$ corresponds to the entanglement of formation of 0.02 ebit within the Holstein-Primakoff approximation [28]. The life time of entanglement of 0.015s is an order of magnitude longer than the best previous results obtained for measurement induced entanglement [15, 16]. The procedures for the measurement of $\Sigma_J(t)$ and for the calibration of the PN are explained in the Methods section and in the Supplementary Information.

Entanglement is created in a quasi steady state rather than in

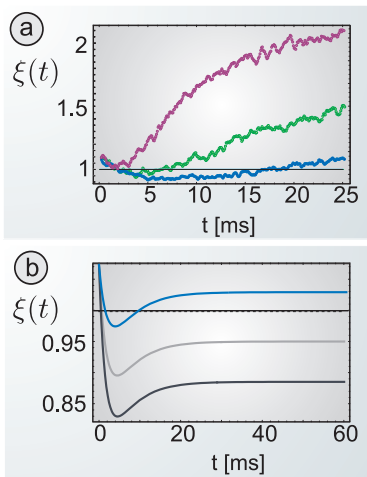


Figure 3: Entanglement in the presence of detuned magnetic fields and strong pump lasers. a) Entanglement for different detunings $\delta\Omega$ of the magnetic fields. Different curves correspond to $\delta\Omega = 0$ (blue), $\delta\Omega = 20\text{Hz}$ (green) and $\delta\Omega = 40\text{Hz}$ (violet). b) Estimated time evolution of $\xi(t)$ in the presence of strong pump and repump fields for $d = 50$, (blue), $d = 100$ (grey) and $d = 150$ (black). For these curves, $\Gamma_{\text{repump}} = \Gamma_{\text{repump}} = 0.16$ was assumed. All other parameters take the same values as in the fits in a) and b). Details can be found in the Supplementary Information.

a steady state, as would be the case for a true two-level atomic ground state, since ^{133}Cs atoms have a multi-level structure. As evident from Fig. 2a,b, in the beginning the evolution of the atomic system is governed by the desired dynamics and quickly reaches a steady state with respect to the two-level subsystem. On a longer time scale of T_1 atoms are lost to the level $F = 3$, which leads to a continuously decreasing population $N_2(t)$ and modified polarization $P_2(t)$ in the relevant two-level subsystem. This leads to the eventual extinction of entanglement as described well by the fits shown in Fig. 2 (see Methods Section and Supplementary Information).

Additional evidence that the entanglement is produced by the collective dissipation process is provided by its dependence on the dephasing between spin coherences of the two ensembles. To demonstrate this dependence we introduce a detuning $\delta\Omega = \Omega_I - \Omega_{II}$ of the Larmor frequencies of the two ensembles by tuning the bias magnetic fields. Fig. 3a shows that already at $\delta\Omega = 20\text{Hz}$ entanglement disappears. This can be understood as a consequence of the "which way" information provided by the distinguishability of the photons scattered from the two ensembles into the sideband modes $\omega_L \pm \Omega_I$ and $\omega_L \pm \Omega_{II}$, separated in frequency space. Hence the atomic samples do not share the same reservoir any more and entanglement disappears.

In conclusion, we observe entanglement generated by dissipation. The entanglement is produced with macroscopic atomic ensembles in a quasi-steady state. Our work paves the way towards creation of extremely long lived steady state entanglement along two possible routes. Firstly, atoms pos-

sessing two-level electronic ground states can be used, for example Ytterbium (^{171}Yb) [29]. In this case, the two-level theory formulated here can be directly implemented, avoiding additional dynamics which cause ξ to increase in time. Alternatively, a true steady state using multi-level ground states can be achieved according to our model [25] for samples with even higher optical depth if pumping and repumping lasers which counteract undesired transfer of atoms to other levels are applied. Fig. 3b shows the predicted time evolution of entanglement for $d = 50; 100; 150$ in the presence of strong pump and repump fields. The other parameters take the same values as in the fit in Fig. 2a. While steady state entanglement can not be created under the present experimental conditions ($d = 50$), this is possible for higher optical depths, which can be obtained, for example, by placing the atoms inside a low finesse optical cavity.

Acknowledgements

We acknowledge support from the Elite Network of Bavaria (ENB) project QCCC and the EU projects COMPAS, Q-ESSENCE and QUEVADIS. C.A.M. acknowledges valuable discussions with K. Hammerer, K.G.H. Vollbrecht and G. Giedke. Contribution of Jelmer Renema to the early stages of the experiment is gratefully acknowledged.

AUTHOR CONTRIBUTIONS

H.K. and K.J. obtained the experimental data with the assistance of J.M.P. W.W. performed preliminary measurements. C.M. developed the theory. J.I.C. and E.S.P. planned and supervised the work.

METHODS

The evolution of the atomic state variance $\Sigma_J(t)$ is monitored via detection of the polarization of the transmitted light. More specifically, the $\cos(\Omega t)$ and $\sin(\Omega t)$ components of the Stokes parameter S_2 measured by polarization homodyne detection [27] are

$$S_{2c/s}^{\text{out}}(t) = \sqrt{\frac{\Phi}{2}} \sqrt{1 - (\mu - \nu)^2 \kappa^2} \quad (1)$$

$$+ \kappa \sqrt{\frac{\Phi}{2FN}} (J_{z/y,I} \mp J_{z/y,II}), \quad (2)$$

where $\Phi/2$ is the shot noise of light. The atomic variance can be reconstructed from the measured light variance $\sigma_{\text{out}}^2 = \text{var}(\frac{S_{2c}}{2\phi})$:

$$\text{var}\left(\frac{J_{y,I} + J_{y,II}}{2J_x}\right) = \frac{1}{\kappa^2} (\sigma_{\text{out}}^2 - \sigma_{\text{in}}^2 (1 - \kappa^2 (\mu - \nu)^2)). \quad (3)$$

$\text{var}(\frac{S_{2s}^{\text{out}}}{2\phi})$ yields the value $\text{var}(\frac{J_{z,I}-J_{z,II}}{2J_x})$. The same method is used in a separate experiment to calibrate the starting point for the atomic noise of the collective spin $\text{var}(\frac{J_{y,I}+J_{y,II}}{2\langle J_x \rangle})$ and $\text{var}(\frac{J_{z,I}-J_{z,II}}{2\langle J_x \rangle})$ in units of PN, as described in the Supplementary Methods.

For our coherent light source, the input light noise $\sigma_{\text{in}}^2 = 1/2$ is the shot noise of light. The coupling constant is given by $\kappa^2 = \frac{1-e^{-2\gamma_s T}}{(\mu-\nu)^2}$ where $\gamma_s \propto J_x \phi$ and T is the pulse duration.

In an ideal two-level model, steady state entanglement with

$$\xi_{2,\infty} = \frac{1}{P_{2,\infty}} \frac{\tilde{\Gamma} + d\Gamma P_{2,\infty}^2 (\mu - \nu)^2}{\tilde{\Gamma} + d\Gamma P_{2,\infty}}, \quad (4)$$

can be produced, where $P_2 = 2\langle J_x \rangle_2 / N_2$ is the atomic polarization and $\tilde{\Gamma}$ is the dephasing rate associated with noise effects. The quantities above are defined with respect to a spin 1/2 system (labelled with the subscript "2"), and can be related to experimentally measured quantities defined with respect to the ground state spin $F = 4$ (see Supplementary Information). In the limit where the entangled quantum state follows the changing particle number and atomic polarization adiabatically, $\xi_2(t)$ is given by $\xi_2(t) = \frac{\Sigma_{J,2}(0)}{2P_2(t)} e^{-(\tilde{\Gamma}+d(t)\Gamma P_2(t))t} + \xi_2^{\text{lt}}(t) \left(1 - e^{-(\tilde{\Gamma}+d(t)\Gamma P_2(t))t}\right)$, with $d(t) = dN_2(t)/N$. The long-time solution $\xi_2^{\text{lt}}(t)$ is given by Eq. (4), where d and P_2 depend on time.

[1] Myatt C. *et al.* Decoherence of quantum superpositions through coupling to engineered reservoirs. *Nature* **403**, 269–273 (2000).
[2] Gleyzes S. *et al.* Quantum jumps of light recording the birth and death of a photon in a cavity. *Nature* **446**, 297–300 (2007).
[3] Hofferberth, S., Lesanovsky, I., Fischer, B., Schumm, T. & Schmiedmayer, J. Non-equilibrium coherence dynamics in one-dimensional Bose gases *Nature* **449**, 324–327 (2007).
[4] Branderhorst, M. *et al.* Coherent control of decoherence. *Science* **320**, 638–643 (2008).
[5] Syassen, N. *et al.* Strong dissipation inhibits losses and induces correlations in cold molecular gases. *Science* **320** 1329–1331 (2008).
[6] Barreiro, J. *et al.* Experimental multiparticle entanglement dynamics induced by decoherence. Preprint at <<http://arxiv.org/abs/1005.1965>> (2010).
[7] Poyatos, J. F., Cirac, J. I. and Zoller, P., Quantum reservoir engineering with laser cooled trapped ions. *Phys. Rev. Lett.* **77**, 4728–4731 (1996).
[8] Kraus, B. and Cirac, J. I. Discrete entanglement distribution with squeezed light. *Phys. Rev. Lett.* **92**, 013602 (2004).
[9] Diehl, S. *et al.* Quantum states and phases in driven open quantum systems with cold atoms. *Nature Physics* **4**, 878–883 (2008).
[10] Kraus, B. *et al.* Preparation of entangled states by quantum Markov processes. *Phys. Rev. A* **78**, 042307 (2008).
[11] Verstraete, F., Wolf, M.M., Cirac, J.I. Quantum computation and quantum-state engineering driven by dissipation. *Nature Physics* **5**, 633–636 (2009).

[12] Briegel, H.-J., Dür, W., Cirac, J. I., and Zoller, P. Quantum Repeaters: The Role of Imperfect Local Operations in Quantum Communication. *Phys. Rev. Lett.* **81**, 5932–5935 (1998).
[13] Duan, L.-M., Cirac, J.I., Lukin, M., and Zoller, P. Long-distance quantum communication with atomic ensembles and linear optics. *Nature* **414**, 413–418 (2001).
[14] Zoller, P. *et al.* Quantum information processing and communication. *Eur. Phys. J. D* **36**, 203–228 (2005).
[15] Kimble, H.J. The quantum internet. *Nature* **453**, 1023–1030 (2008).
[16] Hammerer, K., Sørensen, A.S., and Polzik, E.S. Quantum interface between light and atomic ensembles. *Rev. Mod. Phys.* **82**, 1041–1093 (2010).
[17] Julsgaard, B., Kozhekin, A., and Polzik, E.S. Experimental long-lived entanglement of two macroscopic objects. *Nature* **413**, 400–403 (2001).
[18] Chaneliere, T. *et al.* Storage and retrieval of single photons transmitted between remote quantum memories. *Nature* **438**, 833–836 (2005).
[19] Chou, C.W. *et al.* Measurement-induced entanglement for excitation stored in remote atomic ensembles. *Nature* **438**, 828–832 (2005).
[20] Eisaman, M. *et al.* Electromagnetically induced transparency with tunable single-photon pulses. *Nature* **438**, 837–841 (2005).
[21] Yuan, Z. *et al.* Experimental demonstration of a BDCZ quantum repeater node. *Nature* **454**, 1098–1101 (2008).
[22] Appel, J. *et al.* Mesoscopic atomic entanglement for precision measurements beyond the standard quantum limit. *Proceedings of the National Academy of Sciences* **106**, 10960–10965 (2009).
[23] Gross, C., Zibold, T., Nicklas, E., Esteve, J., and Oberthaler, M.K. Nonlinear atom interferometer surpasses classical precision limit. *Nature* **464**, 1165–1169 (2010).
[24] Riedel, M. F. *et al.* Atom-chip-based generation of entanglement for quantum metrology. *Nature* **464**, 1170–1173 (2010).
[25] Muschik, C. A., Polzik, E. S. and Cirac, J. I., in preparation.
[26] Raymer, M.G., Funk, A.C., Sanders, B.C., and de Guise, H. Separability criterion for separate quantum systems. *Phys. Rev. A* **67**, 052104 (2003).
[27] Wasilewski, W., Jensen, K., Krauter, H., Renema, J., Balabas, M. and Polzik, E.S. Quantum noise limited and entanglement-assisted magnetometry. *Phys. Rev. Lett.* **104**, 133601 (2010).
[28] Wolf, M.M. *et al.* Gaussian Entanglement of Formation. *Phys. Rev. A*, **69**, 052320 (2004).
[29] Takano, T. Fuyama, M. Namiki, R. and Takahashi, Y. *Phys. Rev. Lett.* **102**, 033601 (2009).

SUPPLEMENTARY DISCUSSION

In the following, the derivation of the main theoretical results is outlined and details concerning the fits of the experimental data are provided. A comprehensive and rigorous derivation of the results presented here can be found in [30].

Derivation of the master equation

The interaction of atoms and light illustrated in Fig. 1 can be described by the effective ground state Hamiltonian

$$H = H_A + H_L + H_{\text{int}},$$

where excited states have been eliminated using the fact that the detuning $|\Delta|$ is large compared to the Doppler width δ_{Doppler} and atomic decay rates Γ_{atomic} . Here and in the following, Γ_{atomic} denotes the largest effective rate for atomic ground states including single particle as well as collective rates (see below). $H_A = \Omega (J_{x,I} - J_{x,II})$ accounts for the Zeeman splitting of the atoms in the external magnetic field and $H_L = \int dk \omega_k a_{\mathbf{k}}^\dagger a_{\mathbf{k}}$ is the free Hamiltonian of the light field, where $a_{\mathbf{k}}$ is the annihilation operator of a photon with wave vector \mathbf{k} and frequency ω_k . In a rotating frame, the interaction Hamiltonian is given by

$$\begin{aligned} H_{\text{int}} = & \int_{\Delta\omega_{ls}} d\mathbf{k} \sum_{\lambda_{\mathbf{k}}} g(\mathbf{k}) \left(\mu \sum_{i=1}^N \sigma_{I,i} e^{i\Delta\mathbf{k}r_i} + \nu \sum_{j=1}^N \sigma_{II,j}^\dagger e^{i\Delta\mathbf{k}r_j} \right) a_{\mathbf{k}}^\dagger \\ & + \int_{\Delta\omega_{us}} d\mathbf{k} \sum_{\lambda_{\mathbf{k}}} g(\mathbf{k}) \left(\mu \sum_{i=1}^N \sigma_{II,i} e^{i\Delta\mathbf{k}r_i} + \nu \sum_{j=1}^N \sigma_{I,j}^\dagger e^{i\Delta\mathbf{k}r_j} \right) a_{\mathbf{k}}^\dagger \\ & + H.C., \end{aligned} \quad (\text{S.1})$$

where $\lambda_{\mathbf{k}}$ specifies the the two orthogonal polarizations of the light mode with wave vector \mathbf{k} . The first and second integral cover narrow bandwidths $\Delta\omega_{ls}$ and $\Delta\omega_{us}$ centered around the lower and upper sideband respectively. The atomic operator $\sigma_{I/II,i} = |\uparrow\rangle_{I/II,i} \langle\downarrow|$ refers to a particle in ensemble I/II at position \mathbf{r}_i , $\Delta\mathbf{k} = \mathbf{k}_L - \mathbf{k}$ and \mathbf{k}_L is the wavevector of the applied classical field. $g(\mathbf{k})\mu$ and $g(\mathbf{k})\nu$ denote the effective coupling strengths of the passive (beamsplitter-like) part of the interaction and the active (squeezing) component of the Hamiltonian respectively. The laser field covers a very narrow bandwidth around the central frequency ω_L and is sufficiently off-resonant such that the interaction is well within the dispersive regime and absorption effects can be neglected.

Starting from Hamiltonian (S.1), a master equation of Lindblad form can be derived for the reduced atomic density matrix $\rho(t)$. To this end, the Born Markov approximation is used, which is well justified for optical frequencies. Since the Larmor splitting exceeds well atomic decay rates $\Omega \gg \Gamma_{\text{atomic}}$, the two sideband modes can be treated as

independent baths. The effect of atomic motion gives rise to noise terms and can be included in the master equation in the form of averaged coefficients, where the average in time corresponds to an average in space. This is legitimate in the fast motion limit, where the time scale set by the average velocity of the atoms v is fast compared to the time scale of the radiative decay $\Gamma_{\text{atomic}} \frac{L}{v} \ll 1$. In this case, the emission of light can be described independently of the evolution of atomic positions.

Using the definitions

$$\begin{aligned} A &= \mu \frac{1}{\sqrt{N}} \sum_{i=1}^N \sigma_{I,i} + \nu \frac{1}{\sqrt{N}} \sum_{i=1}^N \sigma_{II,i}^\dagger, \\ B &= \mu \frac{1}{\sqrt{N}} \sum_{i=1}^N \sigma_{II,i} + \nu \frac{1}{\sqrt{N}} \sum_{i=1}^N \sigma_{I,i}^\dagger, \end{aligned}$$

the resulting master equation can be cast in the form

$$\begin{aligned} \frac{d}{dt} \rho(t) &= \frac{1}{2} d \Gamma A \rho(t) A^\dagger + \frac{1}{2} d \Gamma B \rho(t) B^\dagger \\ &+ \frac{1}{2} \Gamma \mu^2 \sum_{i=1}^N \left(\sigma_{I,i} \rho(t) \sigma_{I,i}^\dagger + \sigma_{II,i} \rho(t) \sigma_{II,i}^\dagger \right) \\ &+ \frac{1}{2} \Gamma \nu^2 \sum_{i=1}^N \left(\sigma_{I,i}^\dagger \rho(t) \sigma_{I,i} + \sigma_{II,i}^\dagger \rho(t) \sigma_{II,i} \right) \\ &+ \dots, \end{aligned} \quad (\text{S.2})$$

where Γ is the single particle decay rate and a short hand notation was used. Master equations of Lindblad form $\frac{d}{dt} \rho(t) = \frac{\gamma}{2} (A \rho(t) A^\dagger - A^\dagger A \rho(t)) + H.C.$ with decay rate γ and jump operator A are abbreviated by the expression $\frac{d}{dt} \rho(t) = \frac{\gamma}{2} A \rho(t) A^\dagger + \dots$. d denotes the resonant optical depth of one atomic ensemble. Note that the entangling terms in the first line are enhanced by a factor d , such that for sufficiently optically thick samples, the additional noise terms reflecting thermal motion are small compared to the desired contributions.

Next, additional cooling and heating processes, as well as dephasing are included. The full master equation is given by

$$\begin{aligned} \frac{d}{dt} \rho(t) &= \frac{1}{2} d \Gamma A \rho(t) A^\dagger + \frac{1}{2} d \Gamma B \rho(t) B^\dagger \\ &+ \frac{1}{2} \Gamma_{\text{cool}} \sum_{i=1}^N \left(\sigma_{I,i} \rho(t) \sigma_{I,i}^\dagger + \sigma_{II,i} \rho(t) \sigma_{II,i}^\dagger \right) \\ &+ \frac{1}{2} \Gamma_{\text{heat}} \sum_{i=1}^N \left(\sigma_{I,i}^\dagger \rho(t) \sigma_{I,i} + \sigma_{II,i}^\dagger \rho(t) \sigma_{II,i} \right) \\ &+ \frac{1}{2} \Gamma_{\text{deph}} \sum_{i=1}^N \left(\sigma_{\downarrow\downarrow,I,i} \rho(t) \sigma_{\downarrow\downarrow,I,i} + \sigma_{\downarrow\downarrow,II,i} \rho(t) \sigma_{\downarrow\downarrow,II,i} \right) \\ &+ \dots, \end{aligned} \quad (\text{S.3})$$

with $\sigma_{\uparrow\uparrow, I/II, i} = |\uparrow\rangle_{I/II, i}\langle\uparrow|$ and $\sigma_{\downarrow\downarrow, I/II, i} = |\downarrow\rangle_{I/II, i}\langle\downarrow|$. The noise terms proportional to $\Gamma\mu^2$ and $\Gamma\nu^2$ in Eq. (S.2) have been absorbed in the second and third line of Eq. (S.3) respectively. The last three lines represent single particle processes. Hence they do not feature a collective enhancement factor as the entangling terms in the first line. As shown in [30], Eq. (S.3) includes all terms that need to be taken into account. Collective dephasing terms, as well as collective contributions due to pump and repump fields can be neglected. Similarly, the distance R between the two ensembles does not play a role for $k_L \gg R/L^2$ and $k_L L \gg 1$, where L is the spatial extend of an atomic ensemble. For the experimental setting under consideration this condition is fulfilled.

Calculation of entanglement

Below it is shown how the entanglement measured by the quantity $\xi = \Sigma_J / (2\langle J_x \rangle)$, where $\Sigma_J = \text{var}(J_{y, I} + J_{y, II}) + \text{var}(J_{z, I} - J_{z, II})$, can be determined in the limit $N \gg 1$, assuming that the number of atoms in the two level system N_2 depends on time. For clarity, operators referring to the two level model are labelled with subscript "2". The time derivative of the variance Σ_{J_2} is calculated using Eq. (S.3). By applying the decorrelation approximation $\langle J_{y/z}(t) J_x(t) \rangle_2 \approx \langle J_{y/z}(t) \rangle_2 \langle J_x(t) \rangle_2$ for mean values of products of transverse and longitudinal spins one obtains

$$\begin{aligned} \frac{d}{dt} \Sigma_{J_2}(t) &= -\left(\tilde{\Gamma} + d(t)\Gamma P_2(t)\right) \Sigma_{J_2}(t) \\ &+ N_2(t) \left(\tilde{\Gamma} + d(t)\Gamma P_2(t)^2 (\mu - \nu)^2\right), \end{aligned}$$

where $d(t) = d N_2(t)/N$, $\tilde{\Gamma} = \Gamma_{\text{cool}} + \Gamma_{\text{heat}} + \Gamma_{\text{deph}}$ and $P_2(t) = 2\langle J_x(t) \rangle / (N_2(t))$. For $t \rightarrow \infty$ and $N_2 = N$,

$$\Sigma_{J_2, \infty} = N \frac{\tilde{\Gamma} + d\Gamma P_{2, \infty}^2 (\mu - \nu)^2}{\tilde{\Gamma} + d\Gamma P_{2, \infty}}.$$

Next, the time evolution of the longitudinal spin is considered. Eq. (S.3) yields

$$\begin{aligned} \frac{d}{dt} \langle J_x(t) \rangle_2 &= -(\Gamma_{\text{heat}} + \Gamma_{\text{cool}}) \langle J_x(t) \rangle_2 \\ &+ \frac{N_2(t)}{2} (\Gamma_{\text{cool}} - \Gamma_{\text{heat}}), \end{aligned}$$

such that for constant particle number $N_2 = N$,

$$\langle J_x \rangle_{2, \infty} = \frac{N}{2} \frac{\Gamma_{\text{cool}} - \Gamma_{\text{heat}}}{\Gamma_{\text{cool}} + \Gamma_{\text{heat}}},$$

and therefore

$$\xi_{2, \infty} = \frac{1}{P_{2, \infty}} \frac{\tilde{\Gamma} + d\Gamma P_{2, \infty}^2 (\mu - \nu)^2}{\tilde{\Gamma} + d\Gamma P_{2, \infty}}, \quad P_{2, \infty} = \frac{\Gamma_{\text{cool}} - \Gamma_{\text{heat}}}{\Gamma_{\text{cool}} + \Gamma_{\text{heat}}}$$

in the steady state. In the limit $d \rightarrow \infty$, this equation reduces to $\xi_{2, \infty} = (\mu - \nu)^2$.

The variation of $N_2(t)$ and $P_2(t)$ is slow compared to the evolution of $\Sigma_{J_2}(t)$. In the limit where the entangled quantum state follows the changing particle number and atomic polarization adiabatically, $\xi_2(t)$ is given by

$$\begin{aligned} \xi_2(t) &= \frac{\Sigma_{J_2}(0)}{2P_2(t)} e^{-(\tilde{\Gamma} + d(t)\Gamma P_2(t))t} \\ &+ \frac{1}{P_2(t)} \frac{\tilde{\Gamma} + d(t)\Gamma P_2(t)^2 (\mu - \nu)^2}{\tilde{\Gamma} + d(t)\Gamma P_2(t)} \left(1 - e^{-(\tilde{\Gamma} + d(t)\Gamma P_2(t))t}\right). \end{aligned} \quad (\text{S.4})$$

Comparison of experimental data and theoretical predictions

In the following, experimentally measured quantities are related to the two level model outlined above. The states $|\uparrow\rangle_{I/II} \equiv |4, \pm 4\rangle$ and $|\downarrow\rangle_{I/II} \equiv |4, \pm 3\rangle$ are encoded in the outermost levels of the $F = 4$ manifold of the $6S_{1/2}$ ground state. The essential features of the experiment can be described by means of a simplified model, which allows one to take additional dynamics due to the multilevel character of Cesium into account and involves only the three atomic states $|4, \pm 4\rangle$, $|4, \pm 3\rangle$ and $|h\rangle_{I/II} \equiv |3, \pm 3\rangle$. For the timescales considered here, atomic population in other sublevels can be neglected. The longitudinal spin of each Cesium sample is defined by

$$\begin{aligned} J_x &= \sum_{i=1}^N \sum_{m=-F}^F m |m\rangle_i \langle m| = \sum_{i=1}^N (4|\uparrow\rangle_i \langle \uparrow| + 3|\downarrow\rangle_i \langle \downarrow|) \\ &= \frac{N_2}{2} (P_2 + 7). \end{aligned}$$

The transverse spin component J_y is given by

$$\begin{aligned} J_y &= \frac{1}{2} \sum_{i=1}^N \sum_{m=-F}^F \sqrt{F(F+1) - m(m+1)} (|m+1\rangle_i \langle m| \\ &+ |m\rangle_i \langle m+1|) = 8J_{y, 2}, \end{aligned}$$

such that $\text{var}(J_{y, I} + J_{y, II}) = 8\text{var}(J_{y, I} + J_{y, II})_2 + 7N_{\downarrow}$, where $N_{\downarrow} = \sum_{i=1}^N |\downarrow\rangle_i \langle \downarrow|$ is the population in the level $|4, \pm 3\rangle$. An analogous identity holds for $\text{var}(J_{z, I} - J_{z, II})$. Accordingly,

$$\xi(t) = \frac{8\Sigma_{J_2} + 14N_{\downarrow}(t)}{N_2(t) (P_2(t) + 7)}. \quad (\text{S.5})$$

Since the model is primarily intended to describe qualitatively the physical effects observed in the experiment with very few parameters, we use $\Gamma_{|\uparrow\rangle \rightarrow |h\rangle} \approx \Gamma_{|\downarrow\rangle \rightarrow |h\rangle} = \Gamma_{\text{out}}$ and $\Gamma_{|h\rangle \rightarrow |\uparrow\rangle} \approx \Gamma_{|h\rangle \rightarrow |\downarrow\rangle} = \Gamma_{\text{in}}$ such that

$$\begin{aligned} \frac{d}{dt} N_2(t) &= -(\Gamma_{\text{out}} + 2\Gamma_{\text{in}}) N_2(t) + 2N\Gamma_{\text{in}}, \\ \frac{d}{dt} \tilde{P}_2(t) &= -(\Gamma_{\downarrow\uparrow} + \Gamma_{\uparrow\downarrow} + \Gamma_{\text{out}}) \tilde{P}_2(t) \\ &+ (\Gamma_{\downarrow\uparrow} - \Gamma_{\uparrow\downarrow}) N_2(t)/N, \end{aligned}$$

where $\tilde{P}(t) = P_2(t)N_2(t)/N$ and the abbreviations $\Gamma_{|\uparrow\rangle\rightarrow|\downarrow\rangle} = \Gamma_{\uparrow\downarrow}$ and $\Gamma_{|\downarrow\rangle\rightarrow|\uparrow\rangle} = \Gamma_{\downarrow\uparrow}$ were used. Atomic transitions can be either induced by the driving field or due to collisions. Since the thermal energy of atoms is much larger than the atomic level splittings, we assume the same collisional rate Γ_{col} for all atomic transitions. Accordingly,

$$\begin{aligned}\Gamma_{\downarrow\uparrow} &= \mu^2 \Gamma_L + \Gamma_{\text{col}}, \\ \Gamma_{\uparrow\downarrow} &= \nu^2 \Gamma_L + \Gamma_{\text{col}}, \\ \Gamma_{\text{out}} &= \Gamma_L^{\text{out}} + \Gamma_{\text{col}}, \\ \Gamma_{\text{in}} &= \Gamma^{\text{col}},\end{aligned}$$

where $\mu^2\Gamma_L$ and $\nu^2\Gamma_L$ are the driving field induced cooling and heating rate respectively. Γ_L^{out} is the rate at which atoms leave the two level subsystem due to radiative transitions caused by the driving field. The number of free parameters in these equations can be reduced to two, by measuring the time derivative of the atomic polarization $P = \langle J_x(t) \rangle / \langle J_x(0) \rangle$ at time $t = 0$

$$\left. \frac{d}{dt} P(t) \right|_{t=0} = \frac{-(\Gamma_{\uparrow\downarrow} + 4\Gamma_{\text{out}}) N_{\uparrow}(0) + (\Gamma_{\downarrow\uparrow} - 3\Gamma_{\text{out}}) N_{\downarrow}(0)}{\langle J_x(0) \rangle},$$

where it is taken into account that the initial spin state is not perfectly polarized, but contains a small fraction of atoms in state $|\downarrow\rangle$. The initial populations $N_{\uparrow}(0) = 0.99$, $N_{\downarrow}(0) = 0.01$ and $N_h(0) = 0$ are estimated based on measurements of the orientation of the initial spin state after optical pumping. Using this constraint, $P(t)$ can be fitted with two free parameters. This way, fixed expressions for $P_2(t)$ and $N_2(t)$ are obtained, which can be inserted into Eq. (S.4). The parameters $d\Gamma$ and $\tilde{\Gamma}$ are determined by measuring the slope of the variance $\Sigma_J(t) / (2\langle J_x \rangle)$ at time $t = 0$

$$\begin{aligned}\left. \frac{d}{dt} \frac{\Sigma_J(t)}{2\langle J_x(0) \rangle} \right|_{t=0} &= -4N d\Gamma P_2(0) \left(1 - P_2(0) / (\mu - \nu)^2 \right) \\ &\quad + 7\tilde{\Gamma} P_2(0) - 7(\Gamma_{\text{out}} + \Gamma_{\downarrow\uparrow} - \Gamma_{\uparrow\downarrow}) N_{\downarrow}(0),\end{aligned}$$

and the decay of the transverse spin

$$\langle J_y(t) \rangle = e^{-\frac{1}{2}(\tilde{\Gamma} + d\Gamma \tilde{P}_2(t))t} \langle J_y(0) \rangle.$$

The plot shown in Fig. 3b is obtained by including strong pump and repump fields in the model. This can be done by adding the pump rate Γ_{pump} to the effective cooling rate such that $\Gamma_{\downarrow\uparrow} = \mu^2\Gamma_L + \Gamma_{\text{col}} + \Gamma_{\text{pump}}$ and adding the repump rate Γ_{repump} to Γ_{in} . The effect of these fields on the dephasing rate associated with noise effects can be estimated by adding $2\Gamma_{\text{pump}}$ to $\tilde{\Gamma}$. Repump fields do not have an effect on $\tilde{\Gamma}$.

[30] Muschik, C. A., Polzik, E. S., and Cirac, J. I. in preparation.

SUPPLEMENTARY METHODS

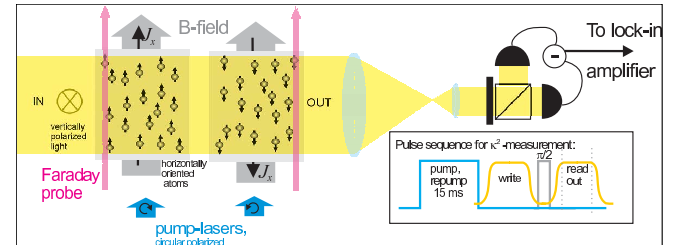
In the following, the experimental methods, which are used to characterize the atomic state are described. This includes the calibration of the coupling constant and the input noise of the transversal spins of the atomic ensembles, as well as the measurement of the orientation of the collective atomic spin.

Projection noise calibration

To characterize the atomic state in the way described in the methods section it is important to know the coupling constant κ .

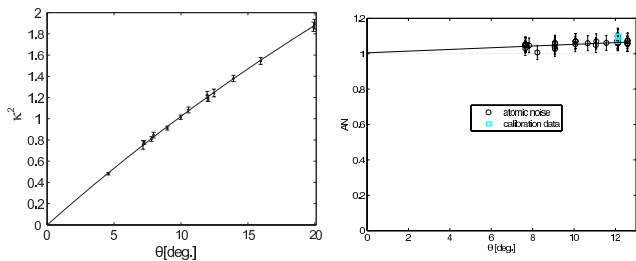
κ^2 can be measured by first mapping onto atoms a 1 ms pulse of light with a known mean value of the Stokes component S_3 , given by the difference of numbers of right hand circular and left hand circular polarized photons. The atomic state readout [31] is performed by observing the cosine and sine modes oscillating at frequency Ω , weighted with the decay of the transversal spin [32]. This is done with an electro-optical modulator which creates a certain average value of S_{3c}^{in} calibrated in the units of shot noise $\sqrt{\Phi}$ by homodyne detection, so that $\langle \frac{S_{3c}^{\text{in}}}{\sqrt{\Phi}} \rangle = C$ is known. The input-output relation for the atomic $\frac{J_{y,I} - J_{y,II}}{\sqrt{2}J_x}$ reads:

$$\begin{aligned}\sqrt{\frac{1}{2J_x}}(J'_{y,I} - J'_{y,II}) &= \sqrt{\frac{1}{2J_x}}(J_{y,I} - J_{y,II}) \sqrt{1 - (\mu - \nu)^2 \kappa^2} \\ &\quad + \kappa \sqrt{\frac{1}{\Phi}} S_{3c}^{\text{in}},\end{aligned}\quad (\text{S.6})$$



Supplementary figure S.1: **Setup and pulse sequence:** The vertically polarized strong probe beam (driving) is sent through the two atomic ensembles with oppositely oriented macroscopic spin. The light state is measured with two detectors in the two output ports of a polarizing beamsplitter, after a half wave-plate. The signals from the detectors are subtracted and sent to a lock-in amplifier, where a certain frequency component is analyzed. The number of atoms is monitored with a weak linearly polarized probe beam, propagating in the direction of the macroscopic spin. The inset shows the pulse sequence for the measurement of κ^2 .

Next $J'_{y,I}$ and $J'_{y,II}$ are rotated into $J_{z,I}$ and $-J_{z,II}$ by momentarily increasing the dc magnetic field. Finally we send a second 1 ms pulse and measure $\langle \frac{S_{3c}^{\text{out}}}{\sqrt{\Phi}} \rangle = \kappa^2 \cdot C$. κ^2 can

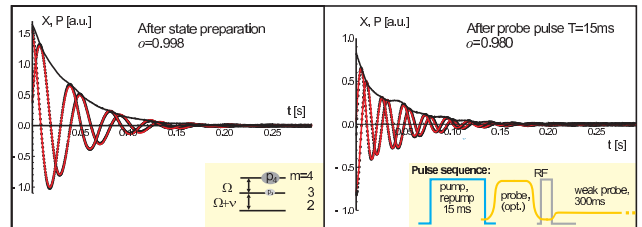


Supplementary figure S.2: κ^2 and atomic noise: κ^2 and atomic noise $\text{AN} = \text{var}\left(\frac{J_{y/z, I \pm J_{y/z, II}}}{2J_x}\right)$ were measured for different Faraday angles $\theta \propto N$, corresponding to different number of atoms N . In both cases, the light power was held constant at 5.6mW, the pulse duration was 1ms. The blue points in the atomic noise graph show the calibration noise points, from the day where the entanglement data presented in the paper was taken. A perfect CSS would have minimum uncertainty noise, meaning $\text{AN} = 1$.

thus be deduced from the ratio $\frac{\langle S_{2c}^{\text{out}} \rangle}{\langle S_{3c}^{\text{in}} \rangle}$. The pulse sequence of this measurement together with a schematic drawing of the experiment is shown in the supplementary figure S.1. The left panel of the supplementary figure S.2 presents the results for the coupling constant measured for different numbers of atoms and a fixed light power of $P = 5.6\text{mW}$. The number of atoms is changed by varying the temperature of the cesium gas.

The scaling of the number of atoms is measured with a weak linearly polarized light beam (Faraday probe) propagating along the direction of the magnetic field. Due to the Faraday effect, the polarization is rotated by an angle θ , which is proportional to the macroscopic spin, and thus the number of atoms for a fully oriented sample. The right panel of the Fig. S.2 presents the reconstructed atomic noise at time zero when the optical pumping is turned off and probe/driving field is turned on, for different θ . The noise is plotted in the units of the projections noise (PN). The figure shows that the initial atomic noise is very close to the PN level, but it is slightly rising for higher atomic numbers, partly due to a small component of classical spin noise in the atoms and partly due to imperfect orientation of the state discussed below. A refined version of Eq. (2) which includes the decay due to spontaneous emission, collisions and spatial gradient of the the magnetic field, and the detection efficiency $\eta = 0.84(3)$ was used for the reconstruction of the atomic noise. The light losses in the detection path which are relevant for the atomic noise reconstruction have been determined in two independent ways. They were measured directly and also inferred from the atomic noise as a function of the atom number. The resulting conservative uncertainty of the atomic noise level 4% mainly originates from the uncertainty in η , κ^2 and the shot noise of light.

The methods described above, characterize the starting point of the entanglement measurement curves, presented in the paper. The points for later times can then be analyzed



Supplementary figure S.3: **Orientation test** for the initial atomic state and after 15ms probing with 5.6mW. The time evolution of a displacement in the two spin components in the rotating frame $X \propto \langle J_y \rangle$ and $P \propto \langle J_z \rangle$ is detected. The black dots are the measurement outcomes and the red lines the fitted curves, from which the orientation o can be determined. The insets show the level structure (with $\nu \approx 20\text{Hz}$) and the pulse sequence. The first probe pulse is optimal.

with Eq. (2). The underlying model, describing the light atom interaction, requires high orientation of the atoms in $F = 4$.

Measurement of the atomic spin orientation

The optimization of the orientation $o = \frac{1}{4} \sum_m m \cdot p_m$, where p_m is the population of the magnetic sub-level m , is crucial for the success of the entanglement generation because significant imperfections of the orientation would lead to the noise above the PN level and because several steps in the theory are only valid for a highly oriented state. In the experiment the orientation as a function of time was measured for the whole probe duration using a method closely related to the method described in [33]. After the preparation of the coherent spin state (CSS) by optical pumping, we use a weak RF magnetic pulse to create excitations, causing a displacement of the rotating collective spin. This displacement is read out with a weak probe beam. The coherences between different magnetic sub-levels oscillate at slightly different frequencies, due to the second order Zeeman shift. In our case this splitting is 20Hz. When we look at the evolution of the displacement demodulated at an RF frequency, close to the Larmor frequency Ω , a population of sub-levels other than $m = 4$ will manifest itself in a beating signal at multiples of the second order Zeeman splitting frequency. In supplementary figure S.3, two signals for slightly different orientations are shown with the difference clearly visible. This method is remarkably sensitive to orientation imperfections. After the pumping, we start very close to the CSS with $o = 0.998(3)$. After a 15ms probe pulse with 5.6mW, the orientation is reduced to $o = 0.980(3)$.

[31] Wasilewski, W., Jensen, K., Krauter, H., Renema, J., Balabas M., and Polzik, E.S. Quantum noise limited and entanglement-assisted magnetometry. *Phys. Rev. Lett.* **104**, 133601 (2010).

[32] The input light modes are defined as $S_{3/2c}^{\text{in}} \propto \int_0^T S_{3/2}^{\text{in}}(t)e^{\gamma_s t} \cos(\Omega t) dt$ and $S_{3s}^{\text{in}} \propto \int_0^T S_{3/2}^{\text{in}}(t)e^{\gamma_s t} \sin(\Omega t) dt$, while the outgoing modes are defined as $S_{3/2c}^{\text{out}} \propto \int_0^T S_{3/2}^{\text{out}}(t)e^{-\gamma_s t} \cos(\Omega t) dt$ and $S_{3s}^{\text{out}} \propto \int_0^T S_{3/2}^{\text{out}}(t)e^{-\gamma_s t} \sin(\Omega t) dt$, where γ_s is the decay constant

of the transversal spin.

[33] Julsgaard, B., Sherson, J., Sørensen, J., and Polzik, E. Characterizing the spin state of an atomic ensemble using the magneto-optical resonance method. *Journal of Optics B* **6**, 5–14 (2004).